# Liquid-Side Ion Exchange Mass Transfer in a Ternary System

Liquid phase mass transfer in a ternary system $[R - A] + (B + E)$ has been analyzed according to the Nernst-Planck equation. The equilibrium isotherm was represented by the mass action law. In the case of $D_A > D_B > D_E$, the resin phase concentration of $B$ ion with time showed a peak. The height of the peak was influenced by the diffusivity ratio, equilibrium constant, and ionic valence. When the modified equilibrium constant $K' \geq 100$ in the case of $A$ ion and $K' \geq 500$ in the case of $B$ and $E$ ions, the exchange rates of the ions could be obtained by approximating $K' = \infty$.

Experimental data on the change of the resin phase concentration $y$ with time are represented. In a $[R - H^+] + (Na^+ + Zn^{2+})$ system, the change of $y_{Na}$ with time showed a high peak. In a $[R - H^+] + (Na^+ + Li^+)$ system, the change of $y_{Li}$ with time showed a small peak. No peaks arose in a $[R - Na^+] + (H^+ + Li^+)$ system. The data agreed reasonably well with the values calculated according to the theoretical equations.

**Takeshi Kataoka, Hiroyuki Yoshida, and Toshifumi Uemura**
Department of Chemical Engineering
University of Osaka Prefecture
Sakai, Osaka 591, Japan

## Introduction

There exists a large number of studies of the liquid-side mass transfer in a binary ion exchange system. The mathematical descriptions for such a system have been presented by many investigators (Copeland et al., 1967; Copeland and Marchellow, 1969; Glasski and Dranoff, 1963; Kataoka et al., 1968, 1971, 1973; Schlögle and Helfferich, 1957; Smith and Dranoff, 1964; Turner and Snowdon, 1968a, b). Schlögle and Helfferich (1957) first applied the Nernst-Planck (N-P) equation to the fluxes of ionic species and showed that the electric field caused by the difference in the diffusivities affects the ion exchange rate significantly. Thereafter the N-P equation has been used for analyzing the kinetics in ion exchange. By comparing the theoretical equations with the experimental data, it has been confirmed that the N-P equation can reasonably be applied to express the rate equation in film diffusion control (Copeland and Marchellow, 1969; Glaski and Dranoff, 1963; Kataoka et al., 1968, 1971, 1973; Smith and Dranoff, 1964; Turner and Snowdon, 1968a, b).

Rahman (1985) presented effective liquid phase diffusivity in a ternary system. However, it has not been clear how the resin phase concentration of each ion and the concentration profile in the liquid film change with time. It is the purpose of this work to develop a theory for a ternary system and to show theoretically how three ions diffuse. We also report the results of an experimental study that was carried out for three typical systems, $[R - Na^+] + (H^+ + Li^+)$, $[R - H^+] + (Na^+ + Li^+)$ and $[R - H^+] + (Na^+ + Zn^{2+})$, in order to test the theory.

Correspondence concerning this paper should be addressed to Hiroyuki Yoshida.

## Theory

Considering the case that $R - A^{Z_A+}$-form resin contacts with $(B^{Z_B+} + E^{Z_E+})(Y_1^{Z_{Y1}-} + Y_2^{Z_{Y2}-})$ solution, the ion exchange reactions are expressed as follows:

$$Z_B R - A^{Z_A+} + Z_A B^{Z_B+} \rightleftharpoons Z_A R - B^{Z_B+} + Z_B A^{Z_A+} \quad (1)$$

$$Z_E R - A^{Z_A+} + Z_A E^{Z_E+} \rightleftharpoons Z_A R - E^{Z_E+} + Z_E A^{Z_A+} \quad (2)$$

$$Z_E R - B^{Z_B+} + Z_B E^{Z_E+} \rightleftharpoons Z_B R - E^{Z_E+} + Z_E B^{Z_B+} \quad (3)$$

Figure 1 shows a conceptual diagram of the concentration profiles in the liquid film.

Applying the Nernst-Planck equation, the fluxes of counterions and noncounterions are given by Eqs. 4 and 5, respectively.

$$J_i = D_i\left(\frac{dC_i}{dr} + \frac{Z_i C_i F}{RT}\frac{d\phi}{dr}\right) \quad (i = A, B \text{ and } E) \quad (4)$$

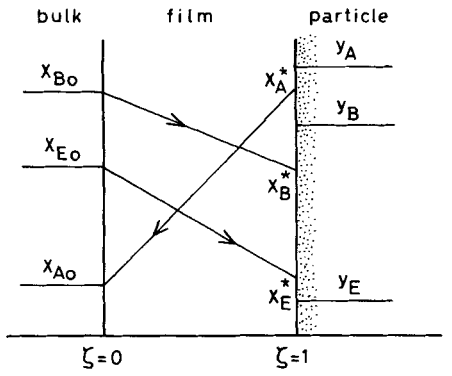


**Figure 1. Conceptual diagram of kinetics in liquid phase diffusion control.**

$$J_j = D_j\left(\frac{dC_j}{dr} - \frac{Z_jC_jF}{RT}\frac{d\phi}{dr}\right) \quad (j = Y_1 \text{ and } Y_2) \tag{5}$$

The conditions of electroneutrality and no net electric current flow in the liquid film are described by Eqs. 6 and 7, respectively.

$$X_A + X_B + X_E = X_{Y_1} + X_{Y_2} \tag{6}$$

$$\Psi_A + \Psi_B + \Psi_E = \Psi_{Y_1} + \Psi_{Y_2} \tag{7}$$

It can be assumed that

$$\Psi_{Y_1} = \Psi_{Y_2} = 0 \tag{8}$$

because of the Donnan exclusion. The dimensionless flux of the counterion is related to the exchange rate by Eq. 9.

$$\Psi_i = \frac{dy_i}{d\tau} \tag{9}$$

where $\Psi_i = Z_iJ_i\delta/D_BC_o$ and $\tau = (D_BC_oa/Q\delta)t$. The condition of the electroneutrality in the resin phase is given by

$$y_A + y_B + y_E = 1 \tag{10}$$

Initial and boundary conditions are shown as follows:

$$\text{IC: } y_A = 1 \text{ and } y_B = y_E = 0; \quad \tau = 0 \tag{11}$$

$$\text{BC: } X_A = X_{Ao}, X_B = X_{Bo} \text{ and } X_E = X_{Eo}; \quad \zeta = 0 \tag{12}$$

$$X_A = X_A^*, X_B = X_B^* \text{ and } X_E = X_E^*; \quad \zeta = 1 \tag{13}$$

The equilibrium relations between $y_i$ and $X_i^*$ are given by the mass action law:

$$\frac{y_BX_A^{*Z_B/Z_A}}{y_A^{Z_B/Z_A}X_B^*} = K_1\left(\frac{Q}{C_o}\right)^{Z_B/Z_A-1} = K_1' \tag{14}$$

$$\frac{y_EX_A^{*Z_E/Z_A}}{y_A^{Z_E/Z_A}X_E^*} = K_2\left(\frac{Q}{C_o}\right)^{Z_E/Z_A-1} = K_2' \tag{15}$$

We next consider the case of equal ionic valences and the case of unequal ionic valences.

### *Ionic valences equal, $Z_A = Z_B = Z_E$ and $Z_Y = Z_{Y_1} = Z_{Y_2}$*

Using Eqs. 4–8 and 12, the relation between $X_A$, $X_B$, and $X_E$ in the liquid film is given by Eq. 16.

$$(X_A + X_B + X_E)(\alpha X_A + X_B + \beta X_E)^{Z_Y/Z_B} = (\alpha X_{Ao} + X_{Bo} + \beta X_{Eo})^{Z_Y/Z_B} \tag{16}$$

where $\alpha = D_A/D_B$ and $\beta = D_E/D_B$. Using Eqs. 6–8 and 16 and boundary condition Eqs. 12 and 13, $\Psi_B$ and $\Psi_E$ are shown by Eqs. 17 and 18, respectively.

$$\Psi_B = \frac{\alpha(1 + Z_B/Z_Y)(X_A^* + X_B^* + X_E^* - 1)}{(1 - \alpha) + (1 - \alpha/\beta)\gamma} \tag{17}$$

$$\Psi_E = \gamma^{\Psi_B} \tag{18}$$

where $\gamma$ is given by Eq. 19.

$$\gamma = \beta\left[\frac{(X_A^* + X_B^* + X_E^*)^{Z_B/Z_Y}X_E^* - X_{Eo}}{(X_A^* + X_B^* + X_E^*)^{Z_B/Z_Y}X_B^* - X_{Bo}}\right] \tag{19}$$

Combination of Eqs. 9, 17, and 18 gives

$$\frac{dy_B}{d\tau} = \frac{\alpha(1 + Z_B/Z_Y)(X_A^* + X_B^* + X_E^* - 1)}{(1 - \alpha) + (1 - \alpha/\beta)\gamma} \tag{20}$$

$$\frac{dy_E}{d\tau} = \gamma\frac{dy_B}{d\tau} \tag{21}$$

Using Eqs. 10 and 14–16, the liquid phase concentrations at the liquid/solid interface are shown as follows:

$$X_A^* = K_1K_2(1 - y_B - y_E)X^{1/(1+Z_Y/Z_B)} \tag{22}$$

$$X_B^* = K_2y_BX^{1/(1+Z_Y/Z_B)} \tag{23}$$

$$X_E^* = K_1y_EX^{1/(1+Z_Y/Z_B)} \tag{24}$$

where

$$X = (\alpha X_{Ao} + X_{Bo} + \beta X_{Eo})^{Z_Y/Z_B} / \{[K_2(1 - K_1)y_B + K_1(1 - K_2)y_E + K_1K_2] \times [K_2(1 - \alpha K_1)y_B + K_1(\beta - \alpha K_2)y_E + \alpha K_1K_2]^{Z_Y/Z_B}\} \tag{25}$$

Solving Eqs. 20 and 21 by using Eqs. 22–25 and the initial condition of Eq. 11, the changes of $y_i$ with time are obtained. The concentration profiles of counterions in the liquid film are given by

$$X_A = \Psi_{A1}(\zeta + 1/\Psi) + \frac{\Psi_{A2}}{(\zeta + 1/\Psi)^{Z_B/Z_Y}} \tag{26}$$

$$X_B = \Psi_{B1}(\zeta + 1/\Psi) + \frac{\Psi_{B2}}{(\zeta + 1/\Psi)^{Z_B/Z_Y}} \tag{27}$$

$$X_E = \Psi_{E1}(\zeta + 1/\Psi) + \frac{\Psi_{E2}}{(\zeta + 1/\Psi)^{Z_B/Z_Y}} \tag{28}$$

where

$$\Psi_{A1} = -\frac{1}{\alpha(Z_B/Z_Y + 1)}\frac{dy_A}{d\tau} \tag{29a}$$

$$\Psi_{B1} = -\frac{1}{(Z_B/Z_Y + 1)}\frac{dy_B}{d\tau} \tag{29b}$$

$$\Psi_{E1} = -\frac{1}{\beta(Z_B/Z_Y + 1)}\frac{dy_E}{d\tau} \tag{29c}$$

$$\Psi = \Psi_{A1} + \Psi_{B1} + \Psi_{E1} \tag{29d}$$

$$\Psi_{A2} = X_{Ao}\Psi^{-Z_B/Z_Y} - \Psi_{A1}\Psi^{-Z_B/Z_Y - 1} \tag{29e}$$

$$\Psi_{B2} = X_{Bo}\Psi^{-Z_B/Z_Y} - \Psi_{B1}\Psi^{-Z_B/Z_Y - 1} \tag{29f}$$

$$\Psi_{E2} = X_{Eo}\Psi^{-Z_B/Z_Y} - \Psi_{E1}\Psi^{-Z_B/Z_Y - 1} \tag{29g}$$

### *Ionic valences not equal*

Applying Eqs. 6–8 to the Nernst-Planck equation, Eqs. 30–32 are obtained.

$$\Psi_A = \frac{dy_A}{d\tau} = -\alpha\left(\frac{dX_A}{d\zeta} + \frac{Z_A X_A}{Z_{Y_1}X_{Y_1} + Z_{Y_2}X_{Y_2}}\frac{dX_T}{d\zeta}\right) \tag{30}$$

$$\Psi_B = \frac{dy_B}{d\tau} = -\left(\frac{dX_B}{d\zeta} + \frac{Z_B X_B}{Z_{Y_1}X_{Y_1} + Z_{Y_2}X_{Y_2}}\frac{dX_T}{d\zeta}\right) \tag{31}$$

$$\Psi_E = \frac{dy_E}{d\tau} = -\beta\left(\frac{dX_E}{d\zeta} + \frac{Z_E X_E}{Z_{Y_1}X_{Y_1} + Z_{Y_2}X_{Y_2}}\frac{dX_T}{d\zeta}\right) \tag{32}$$

where $X_T = X_A + X_B + X_E$. In addition, Eq. 34 is derived by using the Nernst-Planck equation and Eqs. 8 and 33.

$$X_{Y_1} = X_{Bo} \text{ and } X_{Y_2} = X_{Eo}; \quad \zeta = 0 \tag{33}$$

$$\frac{X_{Y_1}^{Z_{Y_2}/Z_{Y_1}}}{X_{Y_2}} = \frac{X_{Bo}^{Z_{Y_2}/Z_{Y_1}}}{X_{Eo}} \tag{34}$$

Equations 30–32 are transformed to finite-difference equations and they are solved simultaneously by using Eqs. 6 and 10–15. The method of the numerical calculation is as follows. Unknown $dy_i/d\tau$ at $\tau + \Delta\tau$ is obtained by trial and error. $dy_B/d\tau$ and $dy_E/d\tau$ are assumed and the concentration profiles of $A$, $B$, and $E$ in the liquid film are calculated. If the concentrations obtained at the liquid/solid interface do not satisfy the equilibrium relation of Eqs. 14 and 15, $dy_B/d\tau$ and $dy_E/d\tau$ are assumed again and the trial-and-error calculation is continued.

Although the exact numerical solutions can be obtained according to the above method, the trial-and-error computation is complicated. To avoid the complexity, the perturbation method is applied. In the case of $Z_{Y_1} = Z_{Y_2} = Z_Y$, Eqs. 30–32 are reduced to Eqs. 35–37, respectively.

$$\Psi_A = -\alpha\left[\frac{dX_A}{d\zeta} + W\frac{X_A}{X_T}\frac{dX_T}{d\zeta} + \epsilon(N - W)\frac{X_A}{X_T}\frac{dX_T}{d\zeta}\right] \tag{35}$$

$$\Psi_B = -\left[\frac{dX_B}{d\zeta} + W\frac{X_B}{X_T}\frac{dX_T}{d\zeta} + \epsilon(M - W)\frac{X_B}{X_T}\frac{dX_T}{d\zeta}\right] \tag{36}$$

$$\Psi_E = -\beta\left[\frac{dX_E}{d\zeta} + W\frac{X_E}{X_T}\frac{dX_T}{d\zeta} + \epsilon(H - W)\frac{X_E}{X_T}\frac{dX_T}{d\zeta}\right] \tag{37}$$

where $N = Z_A/Z_Y$, $M = Z_B/Z_Y$, and $H = Z_E/Z_Y$. $W$ denotes the ratio of the ionic valence of counterion to that of noncounterion in the case that all ionic valences of counterions are equal. $\epsilon$ is the perturbation parameter. When we let

$$X_i = X_{i,0} + \epsilon X_{i,1} + \epsilon^2 X_{i,2} + \cdots \tag{38}$$

and the first two terms of Eq. 38 are used, the following equations are derived.

$$-\frac{\Psi_A}{\alpha}X_{T,0} = X_{T,0}\frac{dX_{A,0}}{d\zeta} + WX_{A,0}\frac{dX_{T,0}}{d\zeta} \tag{39}$$

$$-\Psi_B X_{T,0} = X_{T,0}\frac{dX_{B,0}}{d\zeta} + WX_{B,0}\frac{dX_{T,0}}{d\zeta} \tag{40}$$

$$-\frac{\Psi_E}{\beta}X_{T,0} = X_{T,0}\frac{dX_{E,0}}{d\zeta} + WX_{E,0}\frac{dX_{T,0}}{d\zeta} \tag{41}$$

$$-\frac{\Psi_A}{\alpha}X_{T,1} = X_{T,0}\frac{dX_{A,1}}{d\zeta} + X_{T,1}\frac{dX_{A,0}}{d\zeta} + WX_{A,0}\frac{dX_{A,1}}{d\zeta} + WX_{A,1}\frac{dX_{T,0}}{d\zeta} + (N - W)X_{A,0}\frac{dX_{T,0}}{d\zeta} \tag{42}$$

$$-\Psi_B X_{T,1} = X_{T,0}\frac{dX_{B,1}}{d\zeta} + X_{T,1}\frac{dX_{B,0}}{d\zeta} + WX_{B,0}\frac{dX_{B,1}}{d\zeta} + WX_{B,1}\frac{dX_{T,0}}{d\zeta} + (M - W)X_{B,0}\frac{dX_{T,0}}{d\zeta} \tag{43}$$

$$-\frac{\Psi_B}{\beta}X_{T,1} = X_{T,0}\frac{dX_{E,1}}{d\zeta} + X_{T,1}\frac{dX_{E,0}}{d\zeta} + WX_{E,0}\frac{dX_{E,1}}{d\zeta} + WX_{E,1}\frac{dX_{T,0}}{d\zeta} + (H - W)X_{E,0}\frac{dX_{T,0}}{d\zeta} \tag{44}$$

where

$$X_{T,0} = X_{A,0} + X_{B,0} + X_{E,0} \tag{45}$$

$$X_{T,1} = X_{A,1} + X_{B,1} + X_{E,1} \tag{46}$$

Boundary conditions are given by

$$X_{A,0} = X_{Ao,0},\ X_{B0} = X_{Bo,0} \text{ and } X_{E,0} = X_{Eo,0}; \quad \zeta = 0 \tag{47}$$

$$X_{A,1} = X_{Ao,1},\ X_{B1} = X_{Bo,1} \text{ and } X_{E,1} = X_{Eo,1}; \quad \zeta = 0 \tag{48}$$

The solutions are given by Eqs. 49 and 50.

$$X_{i,0} = \Gamma_i \xi + \frac{\Omega_i}{\xi^W} \tag{49}$$

$$X_{i,1} = \frac{1}{\xi^W} \cdot \left( \Lambda_{i1}\xi^W + \Lambda_{i2}\xi^{W+1} + \Lambda_{i3} \ln|\xi| + \Lambda_{i4}\frac{1}{\xi} + \Lambda_{i5}\frac{1}{\xi^{W+1}} + \Lambda_{i6} \right) \tag{50}$$

Using Eqs. 36, 49, and 50, the liquid phase concentration at liquid/solid interface $X_i^*$ is given by Eq. 51.

$$\begin{aligned} X_i^* &= X_{i,0}|_{\xi=1+\lambda} + X_{i,1}|_{\xi=1+\lambda} \\ &= \Gamma_i(1+\lambda) + \frac{\Omega_i}{(1+\lambda)^W} \\ &\quad + \frac{1}{(1+\lambda)^W}\left[ \Lambda_{i1}(1+\lambda)^W + \Lambda_{i2}(1+\lambda)^{W+1} \right. \\ &\quad + \Lambda_{i3}\ln|1+\lambda| \\ &\quad \left. + \Lambda_{i4}\frac{1}{(1+\lambda)} + \Lambda_{i5}\frac{1}{(1+\lambda)^{W+1}} + \Lambda_{i6} \right] \end{aligned} \tag{51}$$

Equation 51 was solved by using Eqs. 9, 14, and 15 under the initial condition of Eq. 11, and the change of $y_i$ with time was obtained.

## Results of Numerical Computation

### *Ionic values equal, $Z_A = Z_B = Z_E$ and $Z_{Y_1} = Z_{Y_2} = Z_Y$*

Figure 2 shows the effect of $\alpha$ on the exchange rate in the case of $K_1 = K_2 = 1$ and $X_{Bo} = X_{Eo} = 0.5$. The larger $\alpha$, the faster the elution rate of $A$ ion. In the case that $A$ ion is the fastest ion and $B$ ion is faster than $E$ ion, a peak arises in the change of $y_B$ with time. The larger $\alpha$, the higher the peak. When $A$ ion is the fastest, $A$ ion is completely exchanged for $B$ and $C$ ions just after the peak arises. After $A$ ion has disappeared from the particle, $B$ ion sorbed in excess of the equilibrium value is exchanged for $E$ ion until the liquid and the solid phase concentrations of $B$ and $E$ ions reach binary equilibrium.

To investigate these phenomena more closely, concentration profiles and electric potential profiles in the liquid film were obtained. The electric potential profile caused by the difference in the diffusivities is given by Eq. 52.

$$\frac{F\Delta\phi}{RT} = \frac{F(\phi|_\zeta - \phi|_{\zeta=0})}{RT} = \frac{1}{Z_Y}\ln(\Psi\zeta + 1) \tag{52}$$

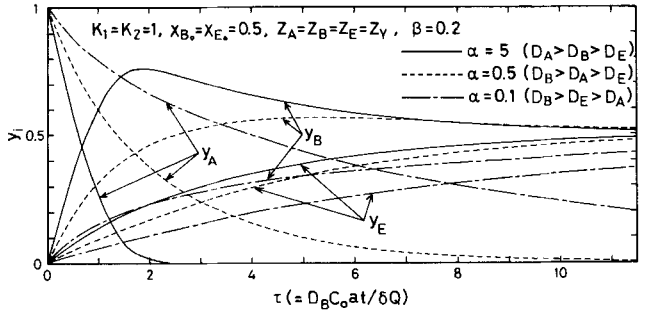


**Figure 2. Effect of $\alpha$ on exchange rate.**

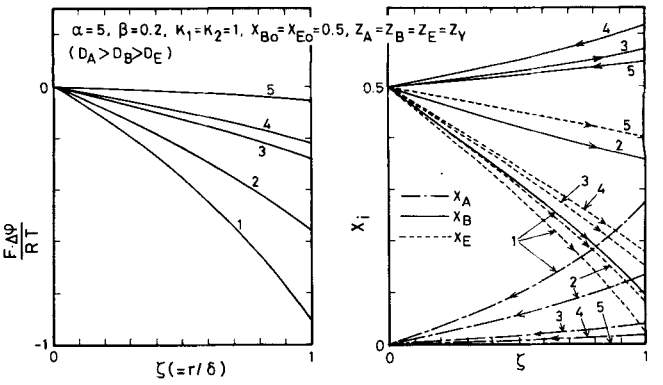


**Figure 3. Electric potential profile and concentration profile in liquid film.**
1. $Y_B = 0.25$, $Y_E = 0.052$
2. $Y_B = 0.625$, $Y_E = 0.143$
3. $Y_B = 0.75$, $Y_E = 0.2$
4. $Y_B = 0.758$, $Y_E = 0.22$
5. $Y_B = 0.575$, $Y_E = 0.425$

Figures 3 and 4 show the results. The Nernst-Planck equation is expressed by

$$\left.\begin{aligned} J_i &= (J_i)_{diff} + (J_i)_{el} \\ (J_i)_{diff} &= -D_i\frac{dC_i}{dr} \\ (J_i)_{el} &= -\frac{Z_i D_i C_i F}{RT}\frac{d\phi}{dr} \end{aligned}\right\} \tag{53}$$

In the case of $\alpha = 5$ and $\beta = 0.2$ $(D_A > D_B > D_E)$, $(J_i)_{el} > 0$ because $d\phi/dr < 0$ as shown in Figure 3a. Therefore, the electric potential accelerates $B$ and $E$ ions and decreases the diffusion rate of $A$ ion. $(J_B)_{el}$ is bigger than $(J_E)_{el}$, because $D_B > D_E$. $B$ ion moves more rapidly than $E$ ion and then it is sorbed more than

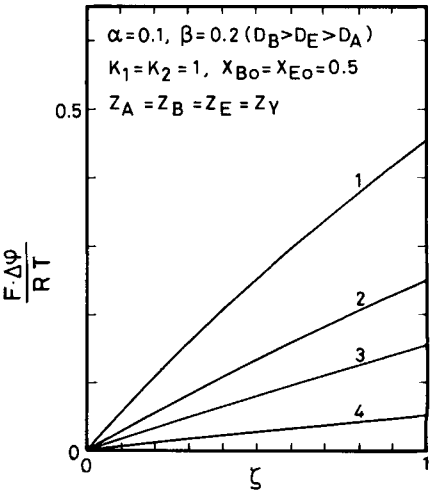


**Figure 4. Electrical potential profile in liquid film.**
1. $Y_B = 0.151$, $Y_E = 0.056$
2. $Y_B = 0.275$, $Y_E = 0.156$
3. $Y_B = 0.351$, $Y_E = 0.251$
4. $Y_B = 0.444$, $Y_E = 0.4$

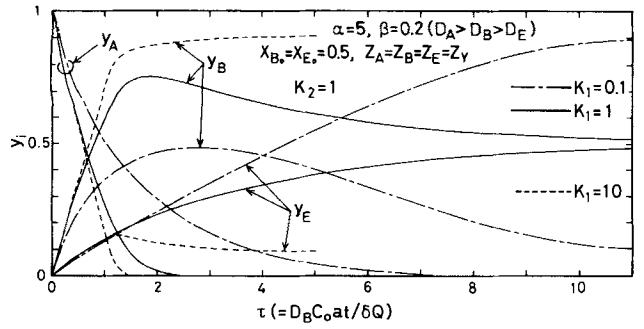


**Figure 5. Effect of $K_1$ on exchange rate.**

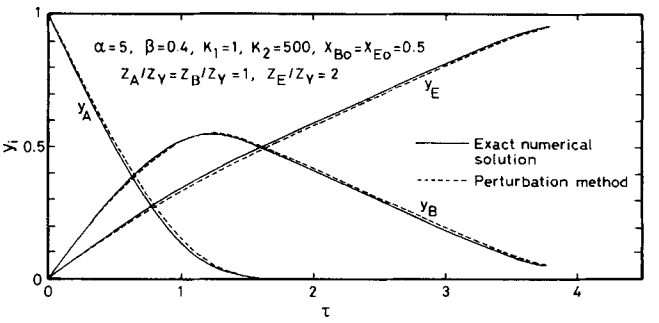


**Figure 7. Comparison of exact numerical solution and solution obtained by perturbation method.**

the equilibrium value. Figure 3b shows such behavior more clearly. $A$ and $E$ ions do not change the direction of the movement during the entire ion exchange process. $B$ ion moves to the resin particle at 1, 2, and 3, and to the bulk solution at 4 and 5. $B$ ion is pumped against the concentration gradient when $X_B^* > X_{B0}$, because $(J_i)_{el} > (J_i)_{diff}$ before the peak. After the peak, as $|(J_i)_{diff}| > |(J_i)_{el}|$ and $(J_i)_{diff} < 0$, $B$ ion moves from the particle to the bulk solution. Figure 4 shows the electric potential profile in the case of $\alpha = 0.1$ and $\beta = 0.2$ ($D_B > D_E > D_A$). The potential profile decreases the diffusion rates of $B$ and $E$ ions and accelerates $A$ ion, because $(J_i)_{el} < 0$. Therefore no peak arises in the change of $y_i$ with time.

Figure 5 shows the effect of $K_1$ on the change of $y_i$ with time in the case of $\alpha = 5$ and $\beta = 0.2$ ($D_A > D_B > D_E$). The larger $K_1$ is, the faster the ion exchange rate of $A$. When $K_1 = 1$ and 0.1, the change of $y_B$ with time shows the peak. When $K_1 = 10$, the peak arises in the change of $y_E$ with time. Figure 6 shows the effect of $K_2$ on the change of $y_i$ with time. The exchange rate of $A$ ion is little affected by $K_2$. When $K_2 = 10$ and 1, the change of $y_B$ with time shows the peak. When $K_2 = 0.1$, the peak arises in the change of $y_E$ with time. These results may show that even in the case of $D_A > D_B > D_E$, no peak arises in the change of $y_B$ with time and a small peak occurs in $y_E$, if $y_B$ at $\tau = \infty$, which is in equilibrium with $X_{Bo}$, is relatively larger than $y_E$ at $\tau = \infty$.

### *Ionic valences not equal*

In Figure 7 the exact numerical solutions of Eqs. 30–32 are compared with the solutions obtained by the perturbation method. There is little difference between them. We obtained several solutions by both methods and the maximum error was 10%. The following solutions were therefore obtained by the perturbation method. The value of $W$ used for the calculation is the nearest integer to the arithmetic mean value of $N$, $M$, and $H$. It minimized the deviation of the perturbation method from the exact solution. When $Z_B \geq 2$ and/or $Z_E \geq 2$ and when $C_o$ is low, $K'$ is large because $K_1' = K_1(Q/C_o)^{Z_B/Z_A - 1}$ and $K_2' = K_2(Q/C_o)^{Z_E/Z_A - 1}$. Many industrial ion exchange operations may satisfy the above conditions. Figures 8–10 show the deviation from the exchange rate for $K' = \infty$ shown by the solid line. It may be seen that the deviation is negligibly small when $K' \geq 100$ in the case of the change of $y_A$ with time and when $K' \geq 500$ in $y_B$. The larger $K_2$ or $K_2'$, (i.e., the smaller $y_B$ at $\tau = \infty$), the sharper the peak. The peak height is little affected by $K_2'$. These phenomena are similar to Figure 6 for $Z_A = Z_B = Z_E$. There is no peak in Figure 9 because $D_B = D_E$ and $K_1' = K_2'$. In Figure 10 ($D_A > D_B > D_E$), a peak occurs in the change of $y_B$ with time. The smaller $K_1'$, the sharper the peak, because the smaller $K_1'$, the smaller $y_B$ at $\tau = \infty$. In Figures 9 and 10, when $K_1'$ and $K_2'$ are large, $y_A$ changes linearly with time, because $X_A^* \simeq 1$ until $y_A$ reaches zero.

Figure 11 shows the effect of $Z_E$ on the exchange rate. The exchange rate of $A$ ion is little affected by $Z_E$. The larger $Z_E$, the faster the exchange rate of $E$ ion and the slower the exchange rate of $B$ ion. This may be clear from Eq. 53: the larger $Z_E$, the larger the acceleration of $E$ ion. Figure 12 shows the effect of $Z_Y$ on the exchange rate. The larger $Z_Y$, the slower the exchange rate of $A$, $B$, and $E$ ions, and the higher the peak of $B$ ion.

## Experimental Procedure

The systems and conditions used in an experimental study are given in Table 1. The equilibrium data were obtained by a batch method. The kinetic data were measured by the single-particle method (Kataoka et al., 1969) and the shallow-bed method. The

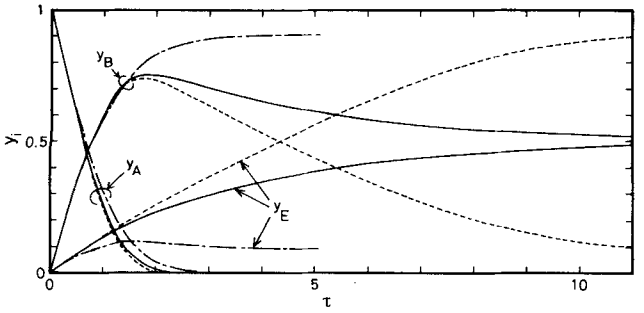


**Figure 6. Effect of $K_2$ on exchange rate.**
$\alpha = 5; \beta = 0.2; X_{Bo} = X_{Eo} = 0.5; Z_A = Z_B = Z_E = Z_Y; K_1 = 1$
$-\cdot-$ $K_2 = 0.1$; — $K_2 = 1$; ····· $K_2 = 10$

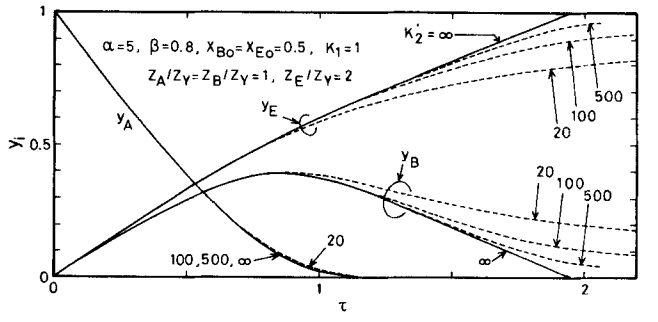


**Figure 8. Effect of $K_2'$ on ion exchange rate.**

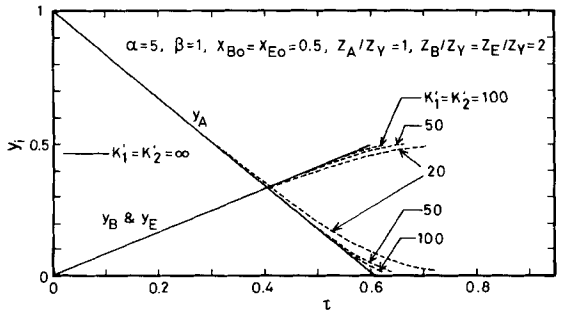


**Figure 9. Effect of $K_2'$ on exchange rate in the case of $K_1' = K_2'$.**

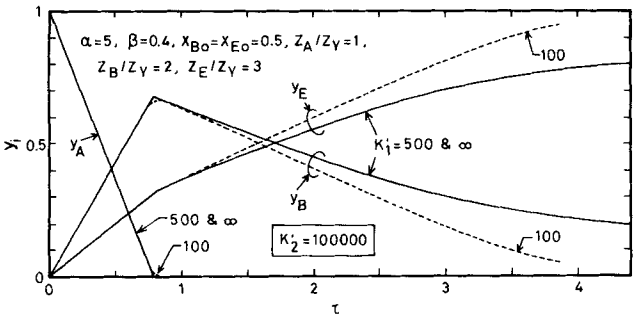


**Figure 10. Effect of $K_1'$ on exchange rate in the case that $K_2'$ is very large.**

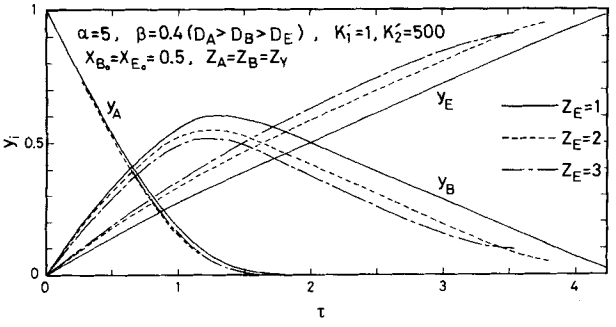


**Figure 11. Effect of $Z_E$ on exchange rate.**

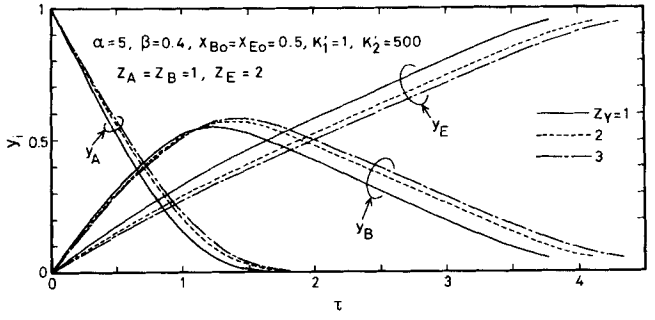


**Figure 12. Effect of $Z_Y$ on exchange rate.**

shallow bed method used in this study is similar to the one that we used for measuring the kinetic data under the condition of intraparticle diffusion control (Kataoka et al., 1977). The shallow bed was formed by putting resin particles between glass beads. The diameter of the glass bead is about the same as that of the resin particle. The shallow bed height is equal to the diameter of the resin particle to prevent a change in the bulk solution concentration. After feeding the solution into the column for a period of time, distilled water was instantaneously supplied and the bed was washed. Thereafter, the ions in the resin phase were desorbed by flowing HCl solution of 1,000 mol/m$^3$. The eluted ions were analyzed by plasma spectroscopy (Spectraspan III) and flame analysis, and the concentrations in the resin phase were evaluated. When $Li^+$ which coexists with $Na^+$ in a solution is analyzed by flame analysis, the absorbance of $Li^+$ is affected by $Na^+$. To avoid this interference, 1 g $La(NO_3)_3$ was dissolved per 100 mL of solution.

In addition, the change of the resin phase concentration with time was also obtained by measuring the solution concentration at the outlet, as described by Tien and Thodos (1960) and Kataoka et al. (1965). An error of about 20% was produced by this method, because it is necessary that the bed height be longer than 3 mm to get the concentration difference at the inlet and outlet of the bed, and this does not satisfy the condition of the constant bulk solution concentration. The error may be caused by axial dispersion while the solution flows through the glass bed under the shallow resin bed. For these reasons, the method mentioned above was adopted. All experiments were conducted at 298 K.

## Results and Discussion

Equilibria in the ternary systems listed in Table 1 were measured under the condition of $C_o = 10$ and $Z_i C_{io} = 5$ (equiv/m$^3$). The data were correlated well by the following equations (Kataoka and Yoshida, 1980). Figure 13 shows the results in the $Na^+ - H^+ - Zn^{2+}$ system. The equilibrium constants were calculated from the slopes of the constants and are listed in Table 2.

$Na^+ - H^+ - Li^+$ System

$$q_H + q_{Li} = Q - \frac{1}{K_{Na-H}} \frac{q_H}{X_H} (1 - X_H - X_{Li}) \qquad (54)$$

$$q_H + q_{Li} = Q - \frac{1}{K_{Na-Li}} \frac{q_{Li}}{X_{Li}} (1 - X_H - X_{Li}) \qquad (55)$$

$Na^+ - H^+ - Zn^{2+}$ System

$$q_H + q_{Zn} = Q - \frac{1}{K_{Na-H}} \frac{q_H}{X_H} (1 - X_H - X_{Zn}) \qquad (56)$$

$$q_H + q_{Zn} = Q - \sqrt{\frac{Q}{K'_{Na-Zn}}} \sqrt{\frac{q_{Zn}}{X_{Zn}}} (1 - X_H - X_{Zn}) \qquad (57)$$

Figures 14–17 show $y_i$ with time in systems I–III (as identified in Table 1). The solid lines are the theoretical results calculated according to theoretical equations derived above, the equilibrium constants in Table 2, and the self-diffusivities in Table 3. The effective liquid film thickness $\delta$ was approximately evalu-

**Table 1. Experimental Systems and Conditions**

| System | Method* | $C_o$ equiv/m$^3$ | $Z_i C_o$ equiv/m$^3$ | Resin |
|---|---|---|---|---|
| I. [$R$-Na$^+$] + (LiCl + HCl) | SB | 10 | 5 | DOWEX 50 WX8 |
| [$R$-$^{22}$Na$^+$] + (LiCl + HCl) | SP | 10 | 5 | $D_p = 6.45 \times 10^{-4}$ |
| II. [$R$-H$^+$] + (LiCl + NaCl) | SB | 10 | 5 | |
| III. [$R$-H$^+$] + [NaCl + Zn(NO$_3$)$_2$] | SB | 10 | 5 | ~$7.00 \times 10^{-4}$m |

*SP, single-particle method; SB, shallow-bed method

ated by Eq. 58 (Kataoka et al., 1972, 1973) and Eq. 59.

$$\left(\frac{1-\epsilon}{\epsilon}\right)^{1/3} \frac{kSc^{2/3}}{u_f/\epsilon} = 1.85\, Re'^{-2/3} \tag{58}$$

$$\delta = \frac{De}{k} \tag{59}$$

where $De$ is a hypothetical effective diffusivity. $De = 2.03 \times 10^{-9}$ m$^2$/s gave the most suitable values of $\delta$, which produced the good agreements between the data and the theoretical values for all systems in this study.

Figure 14 shows $y_i$ with time in system I. The black and white circles for $y_{Na}$ show the data obtained by the single-particle method and the shallow-bed method, respectively. It may be seen that the two methods do not produce any difference. There is no peak in $y_i$ with time in this system, because the fastest ion $H^+$ is in the solution and there is little difference between $\alpha$ and $\beta$ and between $K_1$ and $K_2$. Figure 15 shows the effect of $Re'$ on the change of $y_{Na}$ with time in system I. The data were obtained by the single-particle method. The theoretical lines agree well with the data. These results may suggest that $\delta$ can be estimated according to Eqs. 56 to 58 and 57 to 59.

Figure 16 shows the results in system II. This is an example in which $D_B > D_E$ and $K_1 < K_2$ but the difference in the diffusivities is small and the difference in the equilibrium constants is not so small. As discussed above, a small peak arises in $y_{Li}$ with time, because the selectivity of $Li^+$ is relatively smaller than that of $Na^+$.

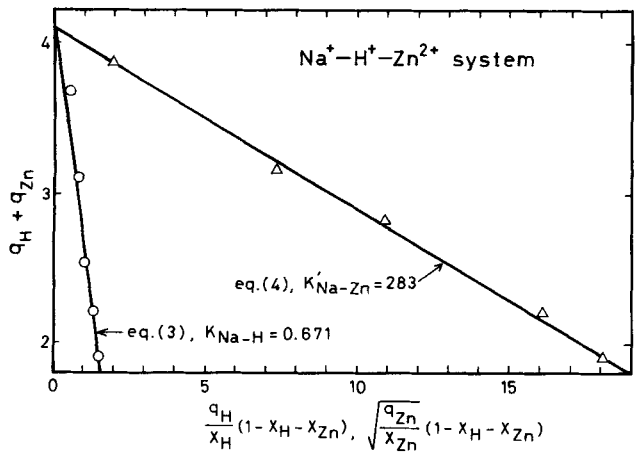


**Figure 13. Arrangement of equilibrium data in [$R$ – Na$^+$] + [HNO$_3$ + Zn(NO$_3$)$_2$] system based on Eqs. 3 and 4.**

$C_o = 10$ equiv/m$^3$; $C_{oH} = 5$; $Z_{Zn}C_{oZn} = 5$

**Table 2. Equilibrium Constants in the Ternary Systems**

| System | Equilibrium Constants |
|---|---|
| [$R$-Na$^+$] + (LiCl + HCl) | $K_1 = K_{Na\text{-}H} = 0.679$<br>$K_2 = K_{Na\text{-}Li} = 0.579$ |
| [$R$-H$^+$] + (LiCl + NaCl) | $K_1 = K_{H\text{-}Li} = 0.879$<br>$K_2 = K_{H\text{-}Na} = 1.47$ |
| [$R$-H$^+$] + [NaNO$_3$ + Zn(NO$_3$)$_2$] | $K_1 = K_{H\text{-}Na} = 1.49$<br>$K'_2 = K'_{H\text{-}Zn} = 629$ |

**Table 3. Diffusivities in the Liquid Phase**

| Ionic Species | Diffusivity m$^2$/s |
|---|---|
| $H^+$ | $9.04 \times 10^{-9}$ |
| $Na^+$ | $1.33 \times 10^{-9}$ |
| $Li^+$ | $1.03 \times 10^{-9}$ |
| $Zn^{2+}$ | $0.712 \times 10^{-9}$ |

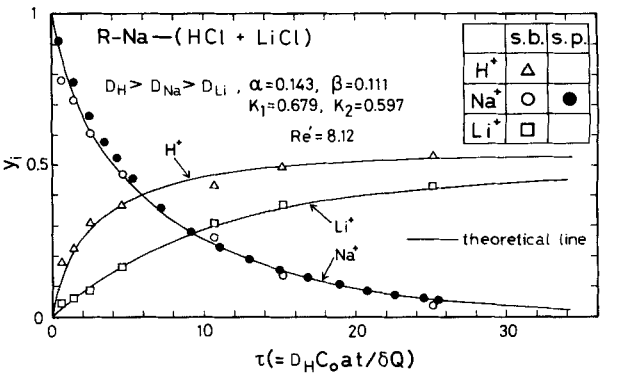


**Figure 14. Change of $y_i$ with time in system I.**

$C_{oH} = 5$; $C_{oLi} = 5$

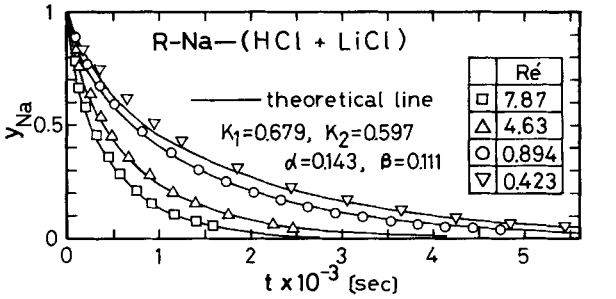


**Figure 15. Effect of $Re'$ on change of $y_i$ with time in system I.**

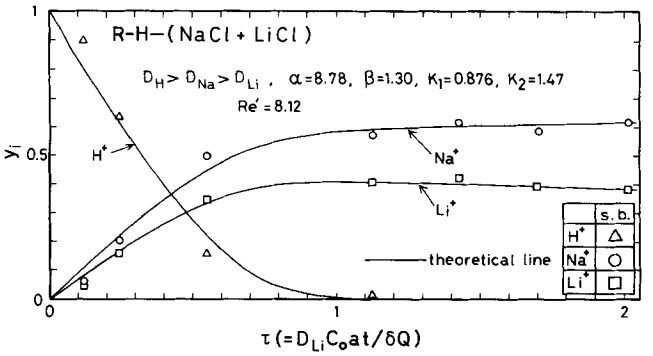


**Figure 16. Change of $y_i$ with time in system II.**
$C_{oLi} = 5$; $Z_{Zn} C_{oZn} = 5$

Figure 17 shows the results in system III. This system is a typical example encountered in an industrial ion exchange operation, namely, the treatment of a solution containing monovalent and multivalent ions by using an H-form ion exchanger. $D_H > D_{Na} > D_{Zn}$ and the differences in the diffusivities are large, as shown in Table 3. Since the difference between $K_1 (= K_{H-Na}) = 1.49$ and $K_2' (= K_{H-Zn}') = 629$ is great, $y_{Na}$ at $\tau = \infty$ is much smaller than $y_{Zn}$ at $\tau = \infty$. We showed above that when the fastest ion is in the resin phase at $\tau = 0$ and $y$ at $\tau = \infty$ of the second fastest ion is much smaller than that of the slowest ion, a sharp peak arises in the change of $y$ of the second fastest ion with time. This is confirmed by Figure 17. A sharp peak occurs in the change of $y_{Na}$ with time. It may be seen that the agreement between the theoretical lines and the data is excellent.

## Notation

$a$ = specific surface area, 1/m
$C$ = liquid phase concentration, mol/m$^3$
$C_o$ = total concentration in bulk solution, equiv/m$^3$
$C_{io}$ = bulk solution concentration of $i$ ion, mol/m$^3$
$C^*$ = liquid phase concentration at solid/liquid interface, mol/m$^3$
$D$ = liquid phase diffusivity, m$^2$/s
$D_e$ = liquid phase hypothetical effective diffusivity, m$^2$/s
$D_p$ = particle diameter, m
$F$ = Faraday's constant
$H = Z_E/Z_Y$
$J$ = flux of ion, mol/m$^2$ · s
$K$ = equilibrium constant
$K_1' = K_1 (Q/C_o)^{Z_B/Z_A - 1}$
$K_2' = K_2 (Q/C_o)^{Z_E/Z_A - 1}$
$k$ = liquid phase mass transfer coefficient, m/s
$M = Z_B/Z_Y$
$N = Z_A/Z_Y$
$Q$ = total exchange capacity, equiv/m$^3$
$q$ = resin phase concentration, mol/m$^3$
$R$ = gas constant
$Re' = D_p u_f \rho/(1 - \epsilon)\mu$, Reynolds number
$r$ = radial dimension, m
$T$ = temperature, K
$t$ = time, s
$u_f$ = superficial velocity, m/s
$W$ = ionic valence ratio
$X_i = Z_i C_i/C_o$
$X_{io} = Z_i C_{io}/C_o$
$X_i^* = Z_i C_i^*/Co$
$y_i = Z_i q_i/Q$
$Z$ = ionic valence

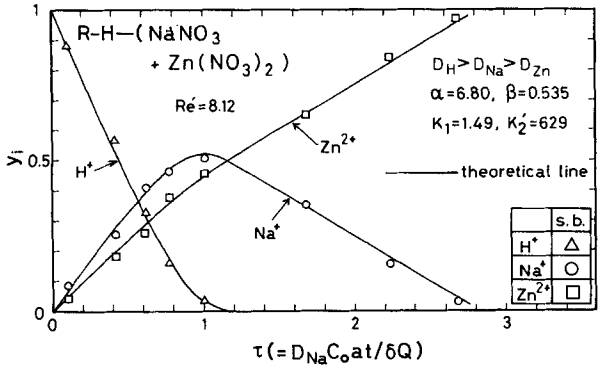


**Figure 17. Change of $y_i$ with time in system III.**
$C_{oNa} = 5$; $Z_{Zn} C_{oZn} = 5$

### Greek letters

$\alpha = D_A/D_B$
$\beta = D_E/D_B$
$\Gamma = \Gamma_A + \Gamma_B + \Gamma_E$
$\Gamma_1 = -(\gamma\Gamma_A + \mu\Gamma_B + \nu\Gamma_E)$
$\Gamma_2 = (\gamma\Omega_A + \mu\Omega_B + \nu\Omega_E)/W$
$\Gamma_3 = X_{To,i} - \Gamma_1\gamma - \Gamma_2\gamma - W$
$\Gamma_A = -\Psi_A/[\alpha(W + 1)]$
$\Gamma_B = -\Psi_B/(W + 1)$
$\Gamma_E = -\Psi_E/[\beta(W + 1)]$
$\gamma = J_E/J_B$
$\delta$ = film thickness, m
$\epsilon$ = perturbation parameter
$\zeta = r/\delta$
$\Lambda_{A1} = -(\Psi_A/\alpha + \Gamma_A)\Gamma_3/W\Gamma$
$\Lambda_{A2} = -\gamma\Gamma_A$
$\Lambda_{A3} = -W\Psi_A\Gamma_2/(\alpha\Gamma) - (N - W)\Omega_A$
$\Lambda_{B1} = -(\Psi_B + \Gamma_B)\Gamma_3/W\Gamma$
$\Lambda_{B2} = -\mu\Gamma_B$
$\Lambda_{B3} = -W\Psi_B\Gamma_2/\Gamma - (M - W)\Omega_B$
$\Lambda_{E1} = -(\Psi_E/\beta + \Gamma_E)\Gamma_3/W\Gamma$
$\Lambda_{E2} = -\nu\Gamma_E$
$\Lambda_{E3} = -W\Psi_E\Gamma_2/[\beta\Gamma - (H - W)\Omega_E]$
$\Lambda_{i4} = -W\Omega_i\Gamma_3/\Gamma$
$\Lambda_{i5} = -W\Omega_i\Gamma_2/\Gamma$
$\Lambda_{i6} = X_{io,1}\lambda - \Lambda_{i1}\lambda^W - \Lambda_{i2}\lambda^{W+1} - \Lambda_{i3}\ln|\lambda| - \Lambda_{i4}a^{-1} - \Lambda_{i5}\lambda^{-W-1}$
$\lambda = X_{To,o}/\Gamma$
$\mu = (M - W)/(W + 1)$
$\nu = (H - W)/(W + 1)$
$\xi = \zeta + \lambda$
$\sigma = (N - W)/(W + 1)$
$\Psi_i = dy_i/d\tau$
$\Omega_A = (X_{Ao,o} - \Gamma_A\lambda)\lambda^W$
$\Omega_B = (X_{Bo,o} - \Gamma_B\lambda)\lambda^W$
$\Omega_E = (X_{Eo,o} - \Gamma_E\lambda)\lambda^W$
$\tau = D_B C_o a t/Q\delta$

### Subscripts

$A$ = counterion species in resin phase at $\tau = 0$
$B$, $E$ = counterion species sorbed from solution
$Y_1$, $Y_2$ = noncounterion species

### Literature cited


Copeland, J. P., C. L. Henderson, and J. M. Marchellow, "Influence of Resin Selectivity on Film-Diffusion-Controlled Ion Exchange," *AIChE J.*, **13**, 449 (1967).

Copeland, J. P., and J. M. Marchellow, "Film-Diffusion-Controlled Ion Exchange with a Selective Resin," *Chem. Eng. Sci.*, **24**, 1471 (1969).

Glaski, F. A., and J. S. Dranoff, "Ion Exchange Kinetics; A Comparison of Models," *AIChE J.*, **9**, 426 (1963).

Kataoka, T., K. Takashima, I. Furuta, and K. Ueyama, "Liquid Phase Mass Transfer in Ion Exchange," *Kagaku Kogaku*, **29**, 368 (1965).

Kataoka, T., M. Sato, and K. Ueyama, "Effective Liquid Phase Diffusivity in Ion Exchange," *J. Chem. Eng. Japan,* **1,** 38 (1968).
———, "Effect of Electric Potential on Liquid Film Diffusion in Ion Exchange," *J. Chem. Eng. Japan,* **31,** 873 (1969).
———, "Influence of a Noncounterion Valence on Liquid Phase Diffusion in Ion Exchange," *Kogyo Kagaku Zasshi,* **74,** 1052 (1971).
Kataoka, T., H. Yoshida, and K. Ueyama, "Mass Transfer in Laminar Region between Liquid and Packing Material Surface in a Packed Bed," *J. Chem. Eng. Japan,* **5,** 132 (1972).
Kataoka, T., H. Yoshida, and T. Yamada, "Liquid Phase Mass Transfer in Ion Exchange Based on the Hydraulic Radius Model," *J. Chem. Eng. Japan,* **6,** 172 (1973).
Kataoka, T., H. Yoshida, and Y. Ozasa, "Breakthrough Curve in Ion Exchange Column—Particle Diffusion Control," *J. Chem. Eng. Japan,* **10,** 485 (1977).
Kataoka, T., and H. Yoshida, "Ion Exchange Equilibria in Ternary System," *J. Chem. Eng. Japan,* **13,** 328 (1980).
Rahman, K., "Effective Liquid Phase Diffusivity in Ion Exchange," *Ind. Eng. Chem. Fundam.,* **24,** 423 (1985).
Schlögle, R., and F. Helferrich, "Comment on the Significance of Diffusion Potentials in Ion Exchange Kinetics," *J. Chem. Phys.,* **26,** 5 (1957).
Smith, T. G., and J. S. Dranoff, "Film-Diffusion-Controlled Kinetics in Binary Ion Exchange," *Ind. Eng. Chem. Fundam.,* **3,** 426 (1964).
Tien, C., and G. Thodos, "Ion Exchange Kinetics: The Removal of Oxalic Acid from Glycol Solution," *Chem. Eng. Sci.,* **13,** 120 (1960).
Turner, J. C. R., and C. B. Snowdon, "Liquid-Side Mass Transfer in Ion Exchange; An Examination of the Nernst-Planck Model," *Chem. Eng. Sci.,* **23,** 221 (1968a).
———, "Liquid-Side Mass Transfer Coefficient in Ion Exchange, the $H^+/Cu^{++} - Cl^-$ System," *Chem. Eng. Sci.,* **23,** 1099 (1968b).

*Manuscript received Mar. 14, 1986, and revision received Aug. 4, 1986.*